Paleobiology, 49(4), 2023, pp. 712–732
DOI: 10.1017/pab.2023.11

PALEOBIOLOGY
A PUBLICATION OF THE Paleontological SOCIETY

Article

Sediment-encased pressure–temperature maturation experiments elucidate the impact of diagenesis on melanin-based fossil color and its paleobiological implications

*Arindam Roy**, *Michael Pittman**, *Thomas G. Kaye*, *and Evan T. Saitta*

Abstract.—Melanin pigments are central to colors and patterns in modern vertebrate integuments, which inform upon ecological and behavioral strategies like crypsis, aposematism, and sociosexual selection. Over the last decade, melanin has emerged as a valuable tool for predicting color in exceptionally preserved fossil feathers and subsequent testing of paleobiological hypotheses in long-extinct dinosaurs and birds. Yet much remains to be learned about melanin stability, diagenetic alterations to melanin chemistry, and their implications for "paleocolor reconstruction." Pressure–temperature maturation experiments with modern feathers offer a way to examine these topics but have mostly been conducted in closed-system capsules or open-system aluminum foil. Both methods have operational limitations and do not consider the filtering effect of porous sediment matrices on thermally labile chemical groups versus stable ones during natural fossilization. We use sediment-encased maturation to resolve this issue and demonstrate replication of organic preservation of melanin highly comparable to compression fossils. Our experiments, coupled with time-of-flight secondary ion mass spectrometry, show predictable volatilization of N/S-bearing molecules and increased melanin cross-linking with elevated temperatures. We also suggest that eumelanin is more stable compared with pheomelanin at higher temperatures, explaining why eumelanic colors (black, dark brown, iridescent) are better preserved in fossils than pheomelanic ones (reddish brown). Furthermore, we propose that proteins preferentially undergo hydrolysis more so than forming N-heterocycles in selectively open systems analogous to natural matrices. Thus, we conclude that melanin pigments and not diagenetically altered protein remnants are the key players in promoting fossilization of soft tissues like feathers.

Arindam Roy†. *Department of Earth Sciences, The University of Hong Kong, Pokfulam, Hong Kong S.A.R., China.* †Present address: School of Earth Sciences, University of Bristol, Wills Memorial Building, Queens Road, Bristol BS8 1RJ, U.K. E-mail: ar15313@bristol.ac.uk

Michael Pittman. School of Life Sciences, The Chinese University of Hong Kong, Shatin, New Territories, Hong Kong S.A.R., China. E-mail: mpittman@cuhk.edu.hk

Thomas G. Kaye. Foundation for Scientific Advancement, Sierra Vista, Arizona 85650, U.S.A. E-mail: tom@tomkaye.com

Evan T. Saitta. Department of Organismal Biology & Anatomy, University of Chicago, Chicago, Illinois 60637, U.S.A. E-mail: evansaitta@gmail.com

Accepted: 14 March 2023
*Corresponding author.

Introduction

Coloration and macroscopic patterning of integumentary structures (skin, scales, feathers, and hair) are closely linked to vertebrate physiology, life history, and behavioral strategies (Burley et al. 1982; Butcher and Rohwer 1989). Coloration is best exemplified in birds (feathers, skin, etc.), as they utilize an astonishing range of pigments to produce complex hues and patterns. Pigment molecules (i.e., biochromes such as carotenoids, melanins, psittacofulvins, and pterins) generate color by preferential reflection of specific wavelengths of light, while others are typically absorbed (Hill and McGraw 2006). It is these wavelengths of reflected light that impart the observable color. "Structural colors" (e.g., iridescent, pearlescent blues) are produced in a special mechanism wherein light is scattered at the interfaces of layered nanoscale arrangements of reflective tissue constituents varying in refractive

0094-8373/23

properties (e.g., keratin granules or melanin in bird feathers) (Hill and McGraw 2006). For a complete understanding of feather components, see Table 1.

Melanin pigments play a vital role within the vertebrate pigmentary system for their involvement in physiological functions (protection from UV radiation, surviving high humidity, immune system functions, and advanced thermal homeostasis), visual signaling (aposematism and crypsis), and natural selection (sexual and social) (Roulin 2014; Cuthill et al. 2017; McNamara et al. 2021). Encased within tiny subcellular vesicles called melanosomes, melanin is also of special paleobiological interest in fossilized organisms due to its inherent resistance to the diagenetic processes that normally degrade comparatively less stable biomolecules (Lindgren et al. 2012; Colleary et al. 2015; Saitta et al. 2018b; Pinheiro et al. 2019; Saitta and Vinther 2019). The high-fidelity preservation of melanized soft tissue anatomy reported in several amniote lineages, including fish, frogs and salamanders, snakes, marine reptiles, pterosaurs, non-avialan dinosaurs, birds, and mammals (Lindgren et al. 2014; Saitta et al. 2018b; Pinheiro et al. 2019; Roy et al. 2019; Yang et al. 2019), from global Konservat-Lagerstätten sites has created a unique window of opportunity to model the original appearance of long extinct animals with high scientific accuracy—a feat previously deemed impossible or speculative. Over the last decade, this has given rise to the cutting-edge subdiscipline of paleobiology called "paleocolor research," which has far-reaching implications for robustly reconstructing the evolution of habitat choice, physiology, and behavior in ancient amniotes (Vinther et al. 2016; Brown et al. 2017; Smithwick et al. 2017; Eliason and Clarke 2018) through deep time.

TABLE 1. Chemical composition of bird feathers based on proximate analyses by (Tesfaye et al. 2017).

Feather components	% by weight
Crude lipids	0.83
Crude fiber	2.15
Crude β-cornified proteins (keratin)	82.36
Ash	1.49
Pigments (melanin in this study; other pigments commonly associated with feathers include carotenoids, psittacofulvins and pterins)	Variable
Moisture content	12.33
Nitrogen-free extract (sugars, starches, and small amounts of other materials)	1.02

Organic staining on fossil soft tissues, melanin chemistry, and melanosome geometry are three key parameters for inferring the colors and patterns in fossil amniotes (Lindgren et al. 2014; Colleary et al. 2015; McNamara et al. 2016; Vinther 2020). The extent of organic staining and the general stain intensity are usually the first markers in exceptionally preserved fossils that inform upon the potential in vivo coloration and macroscopic anatomy of the soft tissues preserved (Saitta et al. 2018b). Melanin chemistry determines which of the two major variants of melanin (i.e., eumelanin or pheomelanin) predominate in the preserved soft tissue, providing a potential indication of the original color (Vinther 2020). Eumelanin is formed by the oxidative polymerization of DHI (5,6-dihydroxyindole) and DHICA (5,6-dihydroxyindole-2-carboxylic acid) (Ito and Wakamatsu 1998). Phaeomelanin is formed by the spontaneous combination of dopaquinone (an aromatic derivative of L-dihydroxyphenylalanine, an intermediate of the tyrosine catabolic pathway) with the sulfur-containing amino acid cysteine to generate 5-S-cysteinyl-DOPA which undergoes further oxidation to become phaeomelanin (Greco et al. 2011).

Melanosome shape (elongate, hyperelongate, spherical, subspherical, platelet, or discoid) and form (solid or hollow) can be used to explain the melanin color categories through statistical models (Vinther 2020). Elongate melanosomes in bird feathers typically contain eumelanin and impart dark brown/black/gray colors, whereas spherical to subspherical melanosomes contain pheomelanin and impart buff to reddish-brown colors. Iridescent colors are typically produced by regular, three-dimensional lattice-like nanostructural arrangement of solid or hollow hyper-elongate, platelet, or discoid melanosomes, whereas non-iridescent structural colors are produced by spongy keratin layers lying above a basal elongate melanosome layer. Both iridescent and non-iridescent color-producing melanosomes predominantly contain eumelanin.

https://doi.org/10.1017/pab.2023.11 Published online by Cambridge University Press

The effect of diagenesis on melanin chemistry is of particular interest to paleocolor reconstruction (McNamara et al. 2013; Colleary et al. 2015; Roy et al. 2019) for several reasons. First, melanosome geometry has been argued to sometimes be altered beyond recognition after extreme levels of diagenesis (Colleary et al. 2015; Brown et al. 2017; Fabbri et al. 2019). This may prevent meaningful prediction of color using statistical modeling of melanosome shape and size, leaving pigment chemistry as the only available reconstruction option (Brown et al. 2017). Gaps in preserved in vivo melanized soft tissues owing to meteoric weathering and other taphonomic variables also requires a better understanding of melanin diagenesis (Roy et al. 2019). Second, gray colors in feathers (Liu et al. 2014) are produced by a mixture of eu- and pheomelanins, which have high shape variablility in melanosomes (Babarović et al. 2019). This means that color prediction using only statistical models of melansome shape may not be sufficiently predictive. Third, there have been reports that melanosome shape is entirely decoupled from integumetary color in non-archosaur amniotes (Eliason et al. 2016). While this hypothesis still needs further scrutiny, melanin chemistry can already be reliably used to elucidate the type of melanin pigments (eumelanin, pheomelanin, or a mixture of both) preserved in non-archosaur amniotes. Thus, a key roadblock in this three-tier system of inferring paleocolor (organic staining, melanin chemistry, and melanosome geometry) is the complex interplay of geobiological processes implicated in fossilization (for an excellent review, see Parry et al. 2018), chief among which is diagenesis. With this fact in mind, this study asks the question: "How does diagenesis of melanin impact our paleobiological understanding of color in fossil organisms?" Actuopaleontological experiments simulating natural taphonomic events under laboratory conditions offer an empirical way to answer this question.

Role of Laboratory-based Experiments in Studying the Taphonomy of Melanized Soft Tissues and the Core Aims of This Study

Controlled laboratory experiments have played pivotal roles in disentangling taphonomic variables that selectively remove, transform, or preserve anatomy and organic biomolecules relevant to paleocolor reconstruction (McNamara et al. 2013, 2018; Purnell et al. 2018; Slater et al. 2020). These experiments focus on specific taphonomic variables while controlling for other potentially confounding ones.

Artificial maturation experiments to simulate late diagenesis of melanin and other molecules usually subject melanized soft tissues to elevated pressure (e.g., $P = 250$ bars) and temperature (e.g., $T = 45°C–300°C$) for comparatively short durations (e.g., hours to days) (Glass et al. 2013; McNamara et al. 2013; Colleary et al. 2015; Saitta et al. 2017, 2018b). The rationale for these treatments lies in chemical kinetics, wherein elevated temperature increases the rate of degradative chemical reactions such that long-term diagenesis under relatively longer, cooler geothermal conditions can be approximated to timescales suitable for laboratory experiments. Typically, P–T-maturation experiments have been conducted using three different methods (Table 2): (1) closed-system capsule maturation (Colleary et al. 2015), which traps both labile and recalcitrant diagenetic products; (2) open-system foil maturation (McNamara et al. 2013), which can lead to uncontrolled loss of both labile and recalcitrant diagenetic products; and (3) sediment-encased maturation (Saitta et al. 2018b), which allows selective retention of stable products and volatilization of labile products through the sediment matrix. Capsule P–T treatments on different melanin types from feathers (black, brown, iridescent, and gray) have revealed that melanosomes undergo isometric shrinkage of about 10–20% due to dehydration and loss of volatile organic components (McNamara et al. 2013; Moyer et al. 2014; Colleary et al. 2015). Chemical changes to melanin during artificial maturation and natural diagenesis have been studied by comparing mass spectra of experimentally matured samples of melanin extract with those of fossils (Lindgren et al. 2010, 2014, 2018; Moyer et al. 2014; Colleary et al. 2015; Clements et al. 2016). Colleary et al. (2015) demonstrated through time-of-flight secondary ion mass spectrometry (ToF-SIMS) and subsequent principal components analysis (PCA) that chemical signatures

https://doi.org/10.1017/pab.2023.11 Published online by Cambridge University Press

TABLE 2. A comparison between capsule and sediment-encased pressure–temperature (P–T) maturation.

Criterion	Capsule maturation	Sediment-encased maturation
Sample placement	Sealed inside inert metal capsules (i.e., totally closed system).	Encased within a compacted, porous sediment matrix (i.e., selectively open system).
Sample size	Capsule diameter <2 mm. Larger samples have alternatively been wrapped in aluminum foil and put into Ar gas–pressurized autoclaves, but the system becomes totally open.	Tissue samples of up to 10–15 mm diameter encased in sediment matrix.
P–T treatment	Inside a water-pressurized autoclave. Al-foil maturation conducted inside Ar gas–powered autoclaves.	Inside an insulated metal chamber with a heating unit (resistor coil/rod) under self-regulated compressed air. Next-generation design of P–T-maturation rig updated from the original study of Saitta et al. (2018b).
Changes in appearance	Often obscured by non-eliminated labile products or altered upon extraction from capsule.	More easily studied due to easy exposure of the sample through splitting of compacted sediment. Stable products are retained within the sediment.
System openness	Sealed capsule traps both labile and recalcitrant molecules produced during maturation. Nonpolar organic solvents (Gupta et al. 2009) can be used to selectively recover recalcitrant molecules of low solubility but may not represent natural conditions and might lead to dissolution and loss of many geochemically relevant compounds (e.g., small aliphatic lipids and sterols).	Porous matrix allows for the filtration of labile, mobile, and volatile molecules produced during maturation, while recalcitrant molecules are retained in a manner more closely approximating natural fossilization conditions.

of tissue-extracted melanin under closed-system capsule maturation show a consistent pattern in which maturation leads to increased chemical similarity toward the mass spectra of fossil samples. However, they did not provide a detailed commentary on the different steps in the chemical transformation of melanin during maturation, and we propose that chemical signatures derived from a combination of labile and recalcitrant molecular fragments trapped within the capsules complicates attempts to do so.

Sediment-encased maturation simulates a more natural approach by embedding whole melanized tissues in a sediment matrix. Saitta et al. (2018b) predicted that sediment-encased maturation provides a selective filter via sediment pores to separate labile from stable compounds, as in natural diagenesis. Their sediment-matured samples showed volume loss in tissues, exposed melanosomes on the sediment, and the production of a dark organic-rich stains from soft tissues while bones persisted. Proteinaceous and fatty tissue morphologies appeared to have been largely lost, as observed by electron microscopy. These results were consistent with capsule maturation showing keratin protein instability (Saitta et al. 2017; Saitta and Vinther 2019) and melanin stability (Colleary et al. 2015), as well as direct analyses of fossil tissues that lack keratin protein (Saitta et al. 2018a) and consist of exposed melanosomes (Nordén et al. 2018). However, the processes underlying these observations have yet to be examined at the chemical level.

Our main goals in this study are to investigate (1) whether melanin diagenesis leads to porosity-mediated selective volatilization of heat-labile molecules while retaining more thermostable ones, (2) whether different melanin types vary in their diagenetic stability, (3) what chemical changes occur to feather constituents (proteins, lipids, and melanin) when subjected to various grades of maturation and how they compare with exceptionally preserved fossils, and (4) the key impacts that different levels of diagenesis have on the process of reconstructing color in fossilized organisms.

We test (1) by hydraulic compaction (8 metric tons) of modern melanized feathers (black, iridescent, gray, and reddish-brown) in porous Ca^{2+}-bentonite clay (exposed to temperatures well below its firing temperature) followed by artificial P–T maturation at a series of temperatures while holding pressure constant (250 bars; approximately 190°C, 200°C, 225°C, 250°C, and 300°C) using a specially fabricated

https://doi.org/10.1017/pab.2023.11 Published online by Cambridge University Press

system (Saitta et al. 2018b). We test (2) by correlating the changes in macroscopic appearance of feather samples after sediment-encased maturation with increasingly higher temperatures and then compare the results with fossils to judge whether the color of the stains in fossils correlates to different degrees of diagenesis. Finally, we answer (3) and (4) by comparing the chemical signature (i.e., ToF-SIMS spectra) of sediment-matured feathers to data of freshly extracted melanin, capsule-matured extracted melanin (200°C and 250°C), and fossil melanized tissues from Colleary et al. (2015), Clements et al. (2016), and Lindgren et al. (2014, 2018). In total, we compile 55 characteristic peaks of melanin from published literature and our experimental samples from sediment-encased maturation of melanized feathers into a comprehensive dataset for a total of 79 samples. This dataset comprises a diverse sampling across geological age (309–20.4 Ma, as well as extant), globally distributed fossil Lagerstätten, tissue types (i.e., ink sacs, skin, feathers, hairs, eyes, and visceral organs), original colors (black, iridescent, brown, and gray; statistically/chemically predicted for fossils as reported in the literature [Colleary et al. 2015]), melanin type (eumelanin, pheomelanin, and mixed), and invertebrate versus vertebrate taxa (for details on sampling/age/locality, see Supporting Information, Table S1, https://doi.org/10.5281/zenodo.7833866).

Materials and Methods

Sample Collection.—Mass spectra of (1) freshly extracted melanin, (2) closed-system capsule-matured extracted melanin, and (3) fossilized melanin were obtained from Colleary et al. (2015) to compare with our sediment-encased maturation of feather subsamples. Additional samples from pennaraptoran dinosaurs *Yi qi* STM 31-2 and *Sapeornis* STM 15-18 were collected from the Shandong Tianyu Museum of Nature in Pingyi, China, and analyzed with ToF-SIMS as part of this study. Naturally shed feathers (black, iridescent, brown, and gray) were collected from U.K.-based poultry farms; the Royal Society for Prevention of Cruelty to Animals (RSPCA) West Hatch Animal Centre in Taunton, U.K.; and the Hong Kong Zoological and Botanical Gardens and Hong Kong Society for Prevention of Cruelty to Animals in China. No animals were harmed in acquiring feather samples, and the samples were collected in accordance with Schedule 1 of the United Kingdom Animals (Scientific Procedures) Act (1986), and Section 15, Wild Animals Protection Ordinance, Agriculture, Fisheries and Conservation Department (AFCD), Hong Kong. For further details on specimens/samples see Supporting Information, Table S1 (https://doi.org/10.5281/zenodo.7833866).

Extraction of Melanin (and Melanosomes) from Feathers.—As stated earlier, we received ToF-SIMS data pertaining to purified melanosome extracts of modern bird feathers (both fresh and capsule matured) from C. Colleary (see "Acknowledgments"), based on previous work by Colleary et al. (2015). The melanosomes were extracted enzymatically using the protocol of Liu et al. (2003) modified by Colleary et al. (2015). The rationale behind this process is to break down the proteinaceous components of the feathers to release the lipid membrane–bound melanosomes using multiple protein degrading enzymes (Proteinase K and Papain). Because melanosomes are enclosed within lipid membranes, they are resistant to this treatment. The steps of the melanosome extraction protocol are as follows: Feather samples were washed with acetone three times to remove any contaminating organic impurities. Next, phosphate buffer (1.5 ml) and dithiothreitol (DTT; 1.5 ml) were added to the samples, then incubated for 24 hours at 37.5°C. DTT breaks the disulfide linkages (–S–S–) in keratin (cornified-β-proteins) and destabilizes the protein chains. Phosphate buffer maintains the pH of the reaction throughout the protocol. Following this, the sample in phosphate buffer was centrifuged (10,000 rpm) to pellet down the cellular debris, proteins, and melanosomes. The pellet was recovered and resuspended in phosphate buffer (15 ml), DTT (5 µl), and Proteinase K (5 mg) and then incubated for an additional 24 hours followed by centrifugation. The resulting pellet was washed with water and phosphate buffer (1.5 ml), after which DTT (15 µl) and Papain (5 mg) were added to each sample,

https://doi.org/10.1017/pab.2023.11 Published online by Cambridge University Press

and samples were then incubated for 24 hours. Following this, the treatment with Proteinase K was repeated with the addition of Triton X-100 (1.5 ml) and the sample was stirred for 4 hours. The Proteinase K treatment was repeated two more times. Proteinase K and Papain are both enzymes that break peptide bonds in proteins, whereas Triton X-100 is an anionic surfactant that breaks down feather waxes. After the last centrifuge step, the resulting pellets containing intact melanosomes were left to dry under a laminar flow hood. These melanosome extracts were used to generate ToF-SIMS spectra.

Hydraulic Compaction.—Sediment-encased P–T maturation comprises two phases: (1) hydraulic compaction of the sample within sediment and (2) P–T maturation. Our method and equipment are modified from those of Saitta et al. (2018b) (Fig. 1). Samples are compacted within sediment using a modified Perkin-Elmer tablet die press (Fig. 1A) consisting of upper and lower interlocking halves, a metal plunger, a metal sealing disk, a sediment tapper (not shown in figure), and a spacer ring. The die press components are first cleaned with 70% ethanol and cotton swabs to remove remaining grit, ensuring a tight seal while preventing jamming of the plunger. The upper half of the die press is inverted, and the spacer ring is first placed around it. The metal plunger and the plastic plunger are subsequently fed through the channel of the die press, leaving enough space to load the sample and surrounding Ca^{2+}-bentonite clay.[1] Ca^{2+}-bentonite is a silicate mineral clay comparable to many fine-grained, fossil-bearing sediments (including those that preserve "exceptional fossils" like feathers) that easily compacts under a hydraulic press for the purposes of our experiments. Approximately half the total amount of the clay is loaded into the channel and leveled with the smooth side of the sediment tapper. Feathers were either cut into small pieces or clipped with a hole puncher to select only the region of the feather with uniform melanin-based color of interest (black, brown, iridescent, or gray). The choice to opt for uniform colors is a logistical one. This is due to the limited diameter of the hydraulic press chamber and the fact that, once thermally matured, it would be difficult to track what barbs were different colors as they all converge to brown stains. So, to ensure that our mass spectra can be traced back to a specific chemistry, we have opted to focus on feathers or regions of feathers without complex color patterns. The feather fragment is placed onto the surface of the clay layer, the remaining half of clay is then loaded over the sample, and the sealing disk is loaded into the channel. A post-maturation split line can be induced by placing foil between the sample and remaining half of the clay before compaction to ensure even splitting of the tablet, and this was used on only four samples in the study (samples 56, 57, 74, and 75; Supporting Information, Table S1, https://doi.org/10.5281/zenodo.7833866). The foil here has been used purely from an "mechanical engineering" point of view as a split line, and there do not appear to be systematic differences between those samples that had the induced split line and those that did not. The lower half of the die press is then united with the top half, and the whole compaction unit is placed under a hydraulic press that drives the metal plunger into the channel, compressing the sediment with a force of 8 metric tons over an area of 126.7 mm^2 (i.e., 62.7×10^6 Pa). Afterward, the upper and lower halves of the die press are separated, the spacer ring is placed between them, and the hydraulic press is used to push the clay tablet out of the channel.

Self-regulated P–T Maturation.—Maturation equipment (Fig. 1B) consisted of an insulated metal pipe with an AC-powered heating rod or AC-powered resistor coil. Some initial low-temperature runs were conducted using a heating rod in contact with the sample chamber, but these failed when attempting temperatures greater than 200°C. The setup was subsequently improved by using a resistive coil instead to attain higher temperatures. Both heaters are directly comparable, given the homeostatic temperature control system. The tablets were loaded into a smaller, metal sample holder (19 mm diameter) positioned inside the larger insulated pipe and attached to a K-type thermocouple temperature sensor. The

[1]Clay was purchased from ClayTerra, Wyoming, U.S.A.

https://doi.org/10.1017/pab.2023.11 Published online by Cambridge University Press

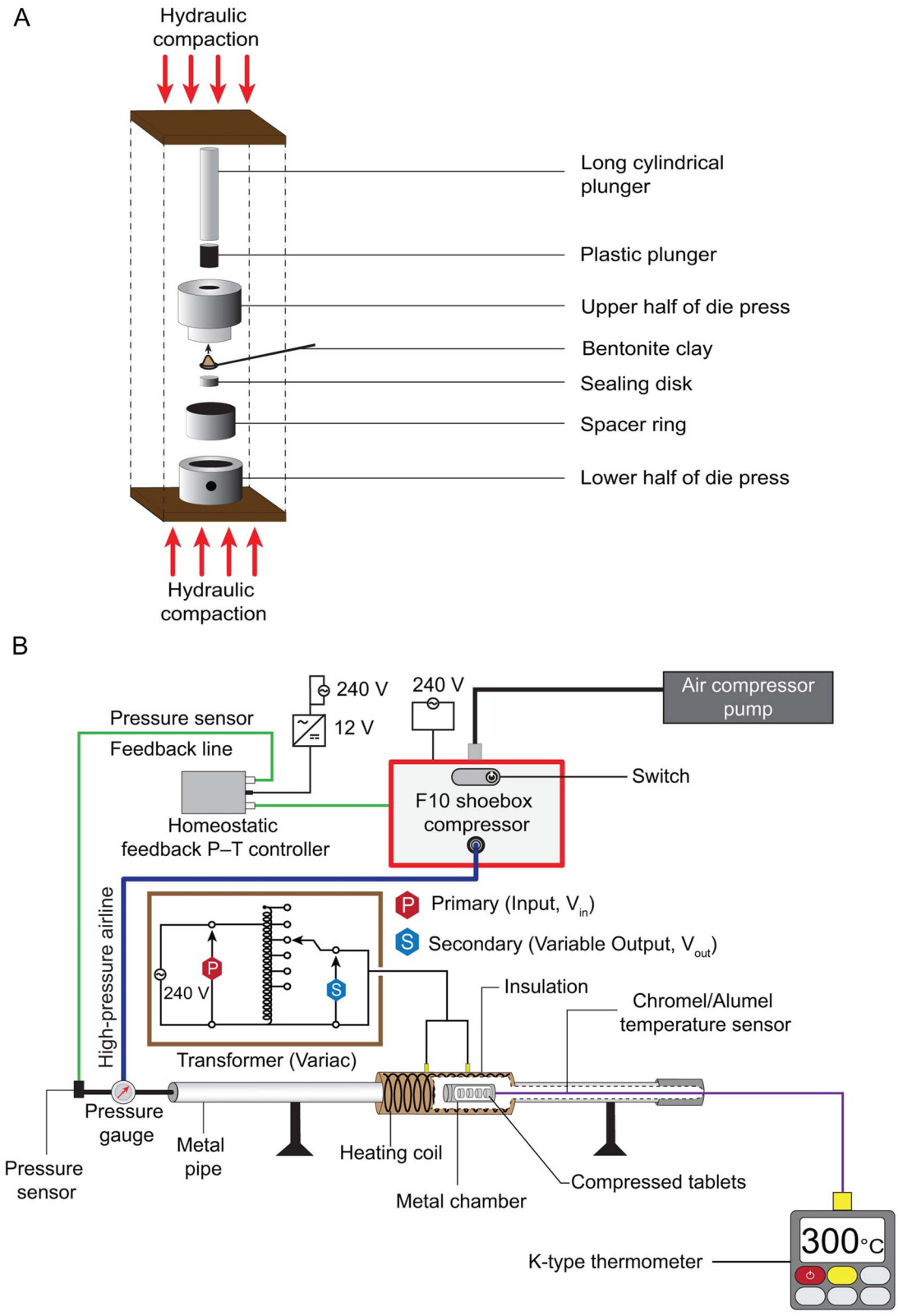

FIGURE 1. Two-part next-generation experimental setup. A, Die press for compaction of samples in sediment. B, Schematic diagram of the pressure–temperature (P–T) maturation rig shown with heating coil setup.

https://doi.org/10.1017/pab.2023.11 Published online by Cambridge University Press

sediment-matured samples were exposed to natural levels of oxygen present in air, because using compressed air is easiest from an engineering perspective to attain pressure in our novel, custom equipment. Note that exceptionally preserved fossils would have likely experienced low, but not necessarily zero, oxygen during their taphonomic history, and future work could improve simulation of natural conditions by altering the air composition of the compressed gas. A high-pressure airline connected a shoebox air compressor to the larger metal pipe. Once the pressure inside the pipe reached 70% of the final pressure, the heater was turned on, and the temperature was calibrated by adjusting the output voltage on the transformer unit. When the final pressure of 250 bars was attained, the temperature and pressure within the metal pipe were maintained in an automated fashion using a digital feedback controller unit connected to the pressure gauge and the shoebox air compressor. Maturation was performed on compacted clay tablets encasing feather samples at 190°C, 200°C, 225°C, 250°C, and 300°C (fluctuation of ±2°C–5°C) with a pressure of 250 bars for 24 hours. The pressure and experimental duration were kept constant to examine the sole effects of temperature on the samples and to control for any extraneous uncertainties introduced into the study. Fossil melanized soft tissues are typically found preserved in low-maturation conditions—maximum organic pyrolysis yield temperature ($T_{max} \leq 435$°C), either before or during very early onset of the oil window (<5500 m depth). For example, squid melanin from Posidonia Shales, Germany (T_{max} < 435°C); Blue Lias, United Kingdom (T_{max} < 411°C–424°C) (Glass et al. 2013); fossil feathers from Crato Formation, Araripe Basin, Brazil (T_{max} < 361°C–433 °C) (Goldberg et al. 2017); and Yixian Formation, Jehol Biota, China (T_{max} < 435°C) (Li et al. 2016). Thus, for our experiment, the lower bound of the temperature range is based on experiments by Colleary et al. (2015), while the upper bound is based on measurements from lowest temperatures in high pressure–high temperature oil wells, illustrating that even relatively hot treatments (e.g., 250°C–300°C) are within the scope of natural conditions to which some fossil organic material can be exposed (Littke et al. 1991; Prauss et al. 1991). Prior work simulating metamorphism (Prauss et al. 1991; Michels and Landais 1994; Marshall et al. 2001; Melenevskii 2012), catagenesis, and metagenesis (Michels and Landais 1994) also informs the chosen upper temperature bound. After each maturation run, the setup was allowed to cool down first and then depressurized. Then, the smaller sample holder and thermocouple temperature sensor were taken out of the metal chamber, and tablets were recovered and glued on their external clay surfaces to aluminum electron microscopy stubs with cyanoacrylate. Finally, most of the pellets were split after maturation by wedging with a razor blade, while a few that split unevenly were further prepped using hand tools (e.g., pin vise).

ToF-SIMS.—The ToF-SIMS parameters chosen were comparable to those of previous work on fossil, modern, and experimental melanin in order for us to combine our data with previously published datasets (Lindgren et al. 2014; Colleary et al. 2015; Clements et al. 2016). An ION-TOF ToF-SIMS V (located at the Materials Characterization and Preparation Facility, Hong Kong University of Science and Technology, Hong Kong SAR, China) was used. The setup used a pulsed (18 ns, 10 kHz) primary ion beam consisting of Bi_3^+ clusters at 30 kV ion energy with low-energy electron flooding for charge compensation. The rationale for choosing polyatomic sputtering (i.e., Bi_3^+ clusters) was to improve the signal by reducing fragmentation of large organic molecules and to be consistent with previous ToF-SIMS data collection (Colleary et al. 2015). Data of high mass resolution were acquired in bunched mode (5000 m/Δm, spatial resolution 0.2–0.3 mm) for experimental and fossil samples (acquired from barbs/barbules in the case of feathers). The ion beam was scanned over areas ranging between 50 and 500 mm^2 at 256 pixels for each sample. The base pressure during spectra acquisition was <1 Å, or 10^{-8} mbar. Mass calibration of ion peaks was conducted by identifying C-cluster peaks from C_1–C_9.

PCA of ToF-SIMS Spectra.—Previously published spectra for melanin reported 55 characteristic negative secondary ion peaks (Lindgren et al. 2012; Colleary et al. 2015;

https://doi.org/10.1017/pab.2023.11 Published online by Cambridge University Press

Clements et al. 2016), and these were used to annotate the TOF-SIMS spectra of unmatured, capsule-matured, and sediment-matured samples as well as fossils. The TOF-SIMS spectra data were compiled into a large dataset and coded according to sample source and treatment category (unmatured, temperature-capsule matured, temperature-sediment matured, and fossil), alongside the mass to charge ratio (*m/z*) values and raw intensity counts (see Supporting Information, Table S1 and Supporting Data, https://doi.org/10.5281/zenodo.7833866). As is then typical for many chemometric studies (ToF-SIMS, Raman, or Fourier transform–infrared spectroscopy), the raw data were then preprocessed (mathematical transformation) before being used with dimensionality-reducing machine learning methods, such as PCA (Cordella 2012; Colleary et al. 2015). Mathematical transformation entailed normalization of raw intensity counts of ion fragments (by dividing each raw intensity count with the total intensity counts for a given spectrum) and mean centering (converting the means of each ion count to zero) using the formula: $-\Sigma(\text{ion count}_i - \mu_{\text{ion count}})$. Preprocessed peak data were then used to perform PCA (variables: sample identity code, treatment category, and transformed peak counts) in JMP v. 14.0 software.

Results

Physical Appearance of Sediment-matured Feathers.—The feather subsamples appear as organic stains and negative impressions in the matrix (Fig. 2B). All samples underwent significant volume loss observable by light microscopy after maturation. Inferences of volume loss are supported by the fact that the areas of compacted matrix originally occupied by feather barbs and barbules have progressively become concave void spaces in the sediment with increasing temperatures. All color categories (black, brown, iridescent, and gray) converge as brown stains under maturation at lower temperatures of 190°C–225°C. Both gray and reddish-brown feathers might show early signs of loss of organic staining at 250°C in the form of lightening of the stain. By 300°C, all samples lose signs of visible, dark organic stains, with the product consisting of negative impressions of the feather structures (i.e., void spaces) in the clay matrix.

PCA of ToF-SIMS Spectra from Unmatured, Fossil, Capsule-, and Sediment-Matured Samples.—The first two principal components explain a total variance of 44.2% (PC 1: 31.6%, PC 2: 12.6%) (Fig. 3). Relatively higher-temperature sediment-matured feathers (250°C) have higher PC 1 scores compared with lower-temperature regimes, indicating enrichment in large N/S fragments (Fig. 4). The 300°C sediment-matured feathers, however, break the observed trend of higher temperatures, tending toward larger PC 1 scores, and appear to revert to the PC 1 origin and otherwise increase in data spread/variability, consistent with a loss of organic carbon.

Unmatured melanin extract has the lowest PC 1 scores, with capsule-matured melanin extract shifting to higher PC 1 scores with increasing temperature. Capsule-matured melanin extract has lower PC 1 scores than sediment-matured feathers, indicating enrichment in smaller N/S fragments in unmatured and capsule-matured melanin than sediment-matured feathers.

Although samples sizes within each temperature category are limited, within each temperature and sample category (i.e., unmatured extract, capsule-matured extract, fossils, and sediment-matured feathers), it seems that high eumelanin concentration tends to have lower PC 1 scores than high pheomelanin concentration (Fig. 5A–G), with gray and non-integumentary mixed (eu- and pheomelanin) samples from visceral organs (eye, liver, etc.) being intermediate. This trend is reversed in the 300°C sediment-matured feathers.

PC 2 is heavily negatively loaded by C_xH^- fragments (Fig. 3B). While fossil samples have PC 1 values spanning from those of capsule-matured melanin extracts (200°C, 250°C) to those of lower-temperature sediment-matured feathers (190°C, 200°C, 225°C), they have higher PC 2 values than all the unmatured modern and experimental samples, indicating lower hydrocarbon (C_xH^-) and carbon skeleton (C_n^-) content in fossils. Loadings of fragments for PC 1–PC4 are tabulated (Table 3) and are shown in Figure S3.

https://doi.org/10.1017/pab.2023.11 Published online by Cambridge University Press

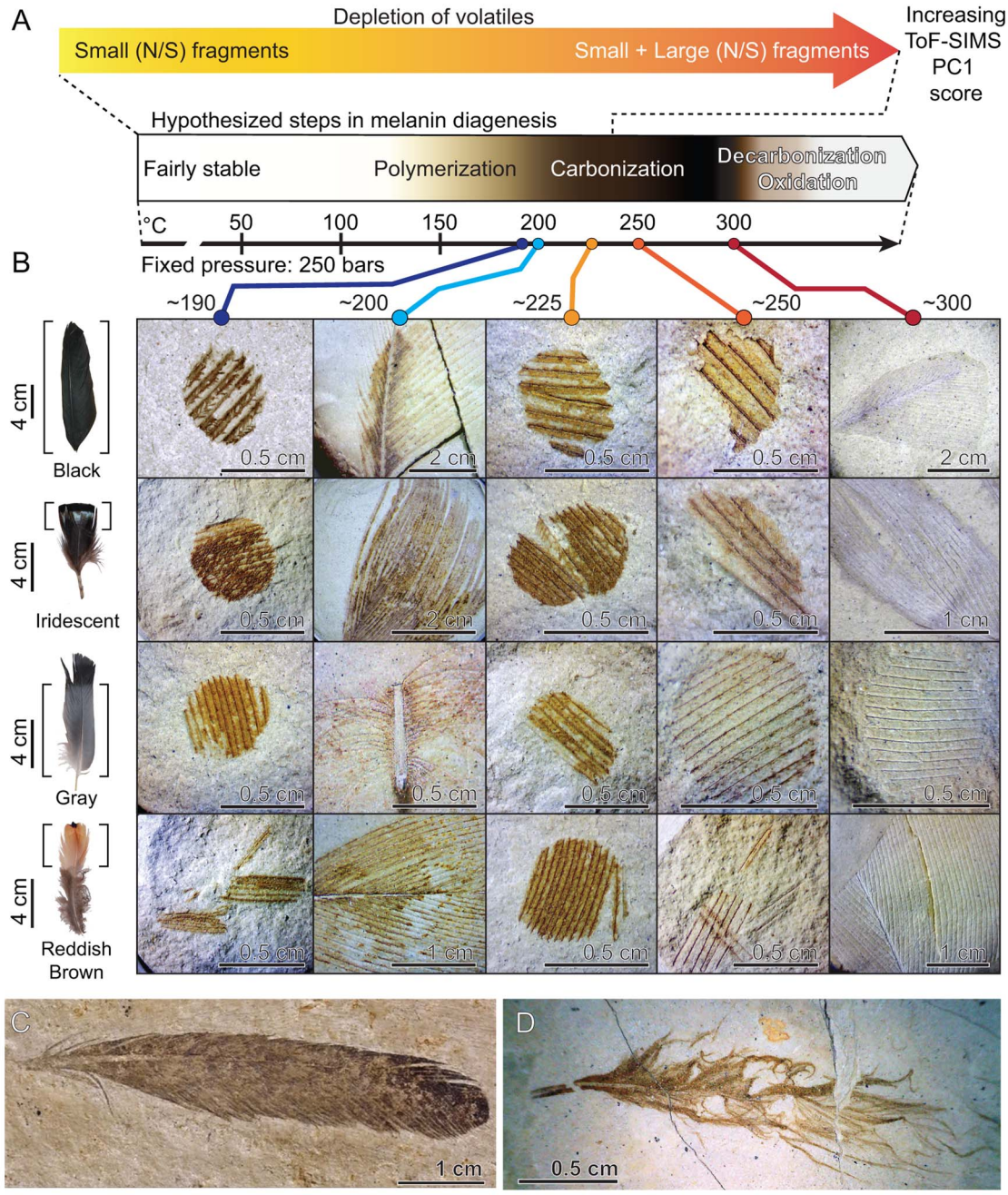

FIGURE 2. Changes in physical appearance of organic staining in sediment-matured samples correlated with chemical changes to melanin during maturation. A, The major changes in melanin chemistry with increase in maturation temperature involve a depletion of small volatile N/S-containing time-of-flight secondary ion mass spectrometry (ToF-SIMS) fragments. This pattern is evidenced by the sequential increase of principal component 1 (PC 1) scores from unmatured (room temperature), aqueous-matured (200°C and 250°C), and sediment-matured samples (up to 250°C). From ToF-SIMS spectra and other published literature, different stages of melanin diagenesis (polymerization, carbonization, and decarbonization/oxidation) were hypothesized to take place over the temperature ranges shown here. B, Changes in physical appearance shown for experimentally matured feathers. Untreated feathers with original color are shown in the left column and different temperature categories shown to the right, revealing brown organic stains in the clay matrix. We predict that diverse melanic colors converge upon brown stains due to cross-linking/polymerization of melanin in the experimental

https://doi.org/10.1017/pab.2023.11 Published online by Cambridge University Press

Discussion

Sediment-encased P–T Maturation Shows That Macroscopic Staining in Fossil Feathers Is Driven by Melanin.—These experiments show that sediment-matured samples are highly comparable to carbonaceous compression fossils from various Lagerstätten in terms of physical appearance and chemistry. Such macroscopic carbonaceous stains inform pigmentation and patterning in fossil taxa (e.g., stripes, mottling, bars, bandit masks, and countershading) (Vinther et al. 2008; Zhang et al. 2010; Smithwick et al. 2017). All feathers in these sediment-based experiments, irrespective of initial color, leave behind brown stains on the bentonite matrix after P–T maturation. The staining appears most intense in the 190°C–225°C treatments and completely disappears at 300°C, leaving behind mainly impressions in the matrix.

The observations have a key paleobiological significance in that they help us to calibrate exceptionally preserved carbonaceous fossils on a scale of increasing diagenetic alteration. Lower temperatures yield samples that resemble fossil feathers from the Mesozoic Altmühltal Formation (Carney et al. 2012), Crato Formation (Vinther et al. 2008; de Souza Carvalho et al. 2015), Jehol Group (Li et al. 2010; Zhang et al. 2010), Koonwarra fossil beds from Australia (Kundrát et al. 2020), as well as the Cenozoic Green River Formation (Thomas et al. 2014) and Fur Formation (Field et al. 2013) (and many other Konservat-Lagerstätten). Note that sediment-matured iridescent feathers leave brown stains on the matrix and do not resemble the fossil feather (SMF ME 3850) with preserved iridescence from the Eocene of the Messel Formation, although this type of original iridescence retention is admittedly rare in fossils (Vitek et al. 2013). Simultaneous unidirectional compaction and P–T maturation would likely be required to preserve original alignment of melanosome layers to preserve iridescence macroscopically in our experiments, because the current method allows melanosomes to settle to the bottom of void spaces left behind as labile components leach into the sediment, losing their original 3D arrangement (Saitta et al. 2018b).

Our work also provides some insight into protein preservation, an active topic of debate for paleoproteomic studies. An appreciable body of prior evidence aligns against preservation of endogenous proteins in ancient carbonaceous compression fossils. Saitta et al. (2018b) showed that sediment-matured samples preferentially lose protein components (evidenced by volume loss of feathers/carcasses and loss of tissue structure under electron microscopy) and retain the now-exposed melanosomes on the sediment matrix. This pattern is also noted in fossils (e.g., Vinther et al. 2008; Li et al. 2010), where only darkly stained striped sections of feathers preserve exposed melanosome films, whereas unpigmented sections show only sediment matrix without any proteinaceous ultrastructural features. If proteins were to survive (relatively intact or cross-linked with sugars or lipids), then presumably, organic mass in the feather tissue would not be significantly lost, and melanosomes would be obscured by these polymers (Vinther 2020). Total ion pyrochromatograms by both Saitta et al. (2017) and Cincotta et al. (2020) showed a lack of enriched peaks resulting from the pyrolysis of modern feather protein in P–T-matured and fossil samples. ToF-SIMS spectra of our experimental samples and fossils are quite different from α- and β-keratin controls from Schweitzer et al. (2018) (see Supporting Information, Fig. S2, https://doi.org/10.5281/zenodo.7833866).

Our results likely contrast with the alternative view in some paleoproteomic studies suggesting that brown organic stains in fossils can be predominantly driven by remnant

FIGURE 2. (*Continued*) temperature range of 190°C–225°C, coinciding with volatile loss. Increased charring/carbonization of the molecule occurs when approaching 250°C, followed by decarbonization/oxidation (i.e., complete loss of organic carbon in the form of CO_2 gas) when approaching 300°C. Exceptional preservation is hypothesized to occur within a small window between 150°C and 250°C. Our low-temperature matured feathers closely resemble fossil feathers in terms of both chemistry and appearance, as exemplified in C. C, Isolated pennaraptoran feather (MB.Av.100) from the Late Jurassic Solnhofen Limestone (Kaye et al. 2019). D, Isolated pennaraptoran feather (IVPP V15388B) (Zhang et al. 2010) from the Early Cretaceous Jehol Group.

https://doi.org/10.1017/pab.2023.11 Published online by Cambridge University Press

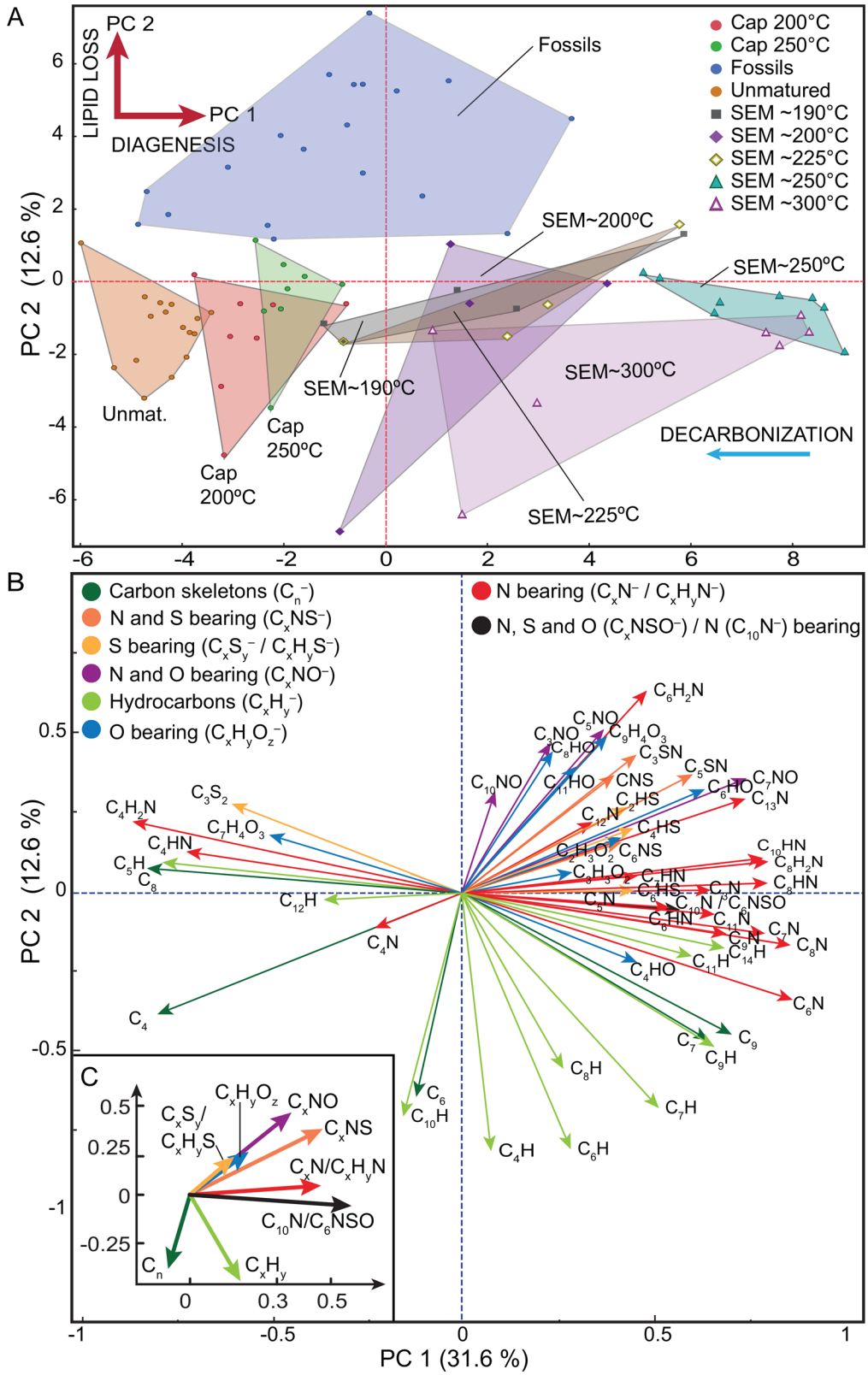

https://doi.org/10.1017/pab.2023.11 Published online by Cambridge University Press

FIGURE 3. A, Principal component analysis (PCA) of time-of-flight secondary ion mass spectrometry (ToF-SIMS) data of fossil and experimental samples. Comparison of secondary ion spectra of fresh melanin extracts, capsule-matured melanin extracts, sediment-encased maturation (SEM) of whole feathers, and fossil samples. Experimental samples sort along PC 1, which describes the pressure–temperature (P–T)-maturation/diagenetic continuum. Sediment-matured samples at 300°C appear to show a reversal toward decreasing PC 1, indicating decarbonization. For a more detailed PCA with sample descriptions, see Supporting Information, Table S1 and Fig. S1A (https://doi.org/10.5281/zenodo.7833866). B, Loading plot indicating the relative contributions of secondary ion fragments on PC 1 and PC 2. The black arrow indicates an ambiguous fragment that is either C_6NSO^- (m/z = 134.00) or $C_{10}N^-$ (m/z = 133.97). Remaining chemical groups of ion fragments are indicated by colors (see key on figure). C, Average loadings of chemical groupings of ion fragments with each chemical group indicated by the color noted in B. For detailed descriptions of chemical fragment descriptions, see Table 3.

proteinaceous components oxidatively condensing with sugar/lipid moieties to yield N-linked melanoidin-like heterocyclic polymers (i.e., advanced glycation end products [AGE] and advanced lipooxidation end products [ALE]) (Wiemann et al. 2020), supporting the value of organic staining as a reliable indicator criterion for melanin-based fossil color interpretation in carbonaceous compression integumentary fossils. Wiemann et al. (2018) conducted their experiments at low temperatures (45°C–120°C) for short durations (10 minutes–1 hour) and did not elevate pressure. Vaporization and removal of water from the hotplate-heated samples of Wiemann et al. (2018) likely promoted condensation reactions between biomolecules (Hodge 1953), enhancing AGE and ALE formation. Drying of tissues during maturation experiments is not realistically representative of typical burial environments preserving keratinous integumentary structures (i.e., extensively waterlogged, reducing lacustrine or marine settings) (Saitta and Vinther 2019). In contrast, the use of a pressurized setup in this study inhibits intrinsic "tissue constituent" water in the feathers from boiling

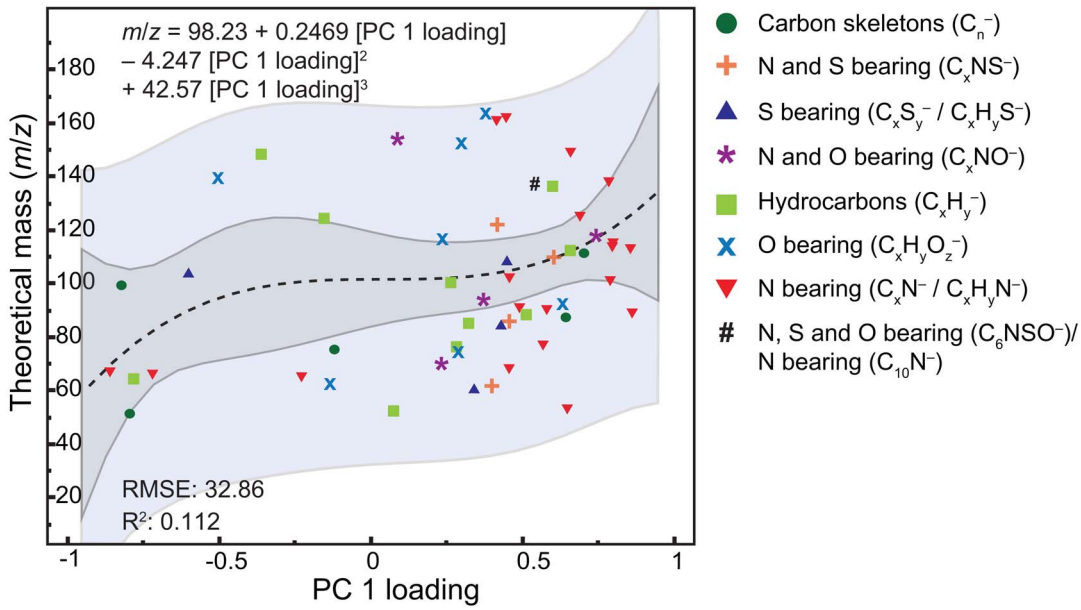

FIGURE 4. Patterns of volatile loss inferred from principal component analysis (PCA). Plot of theoretical mass of secondary ion fragments against their PC 1 loadings indicating that certain fragments with smaller masses are enriched at lower temperatures and in closed systems (i.e., negative PC 1 loadings), whereas these fragments become depleted at higher temperatures and in open systems. Confidence and prediction intervals are represented by darker and lighter shades of gray, respectively. Fragments with higher masses tend to have higher/positive PC 1 loadings. This suggests a progressive loss of small, volatile organics under higher temperatures and sediment pore filtration, while more recalcitrant organics polymerize/cross-link. Capsule maturation traps volatiles normally lost in sediment-encased maturation.

https://doi.org/10.1017/pab.2023.11 Published online by Cambridge University Press

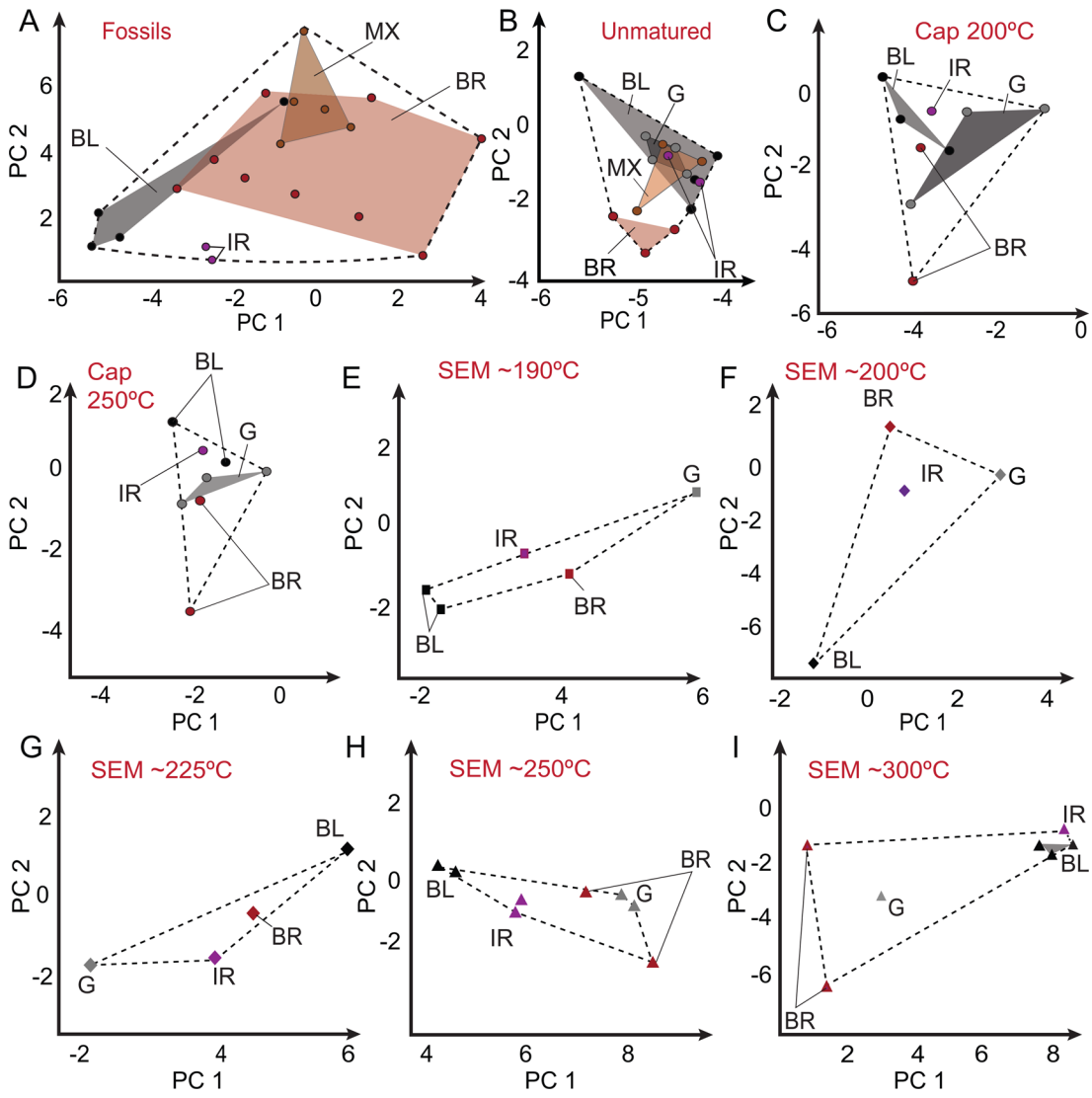

BL: Black, BR: Brown, G: Gray, IR: Iridescent, MX: Mixed

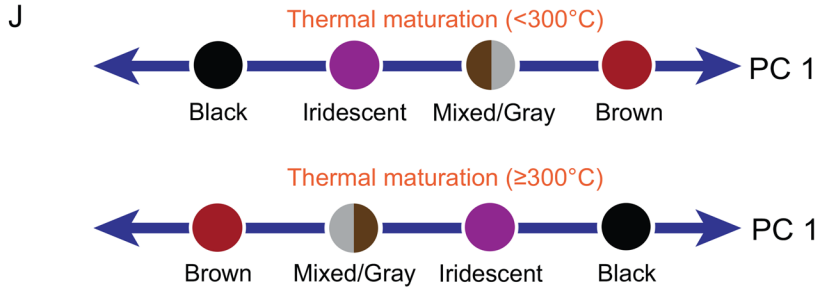

Hypothetical Diagenetic Shift in Melanin Chemistry

https://doi.org/10.1017/pab.2023.11 Published online by Cambridge University Press

FIGURE 5. Same principal component analysis (PCA) as in Fig. 3A but with the different experimental categories, and melanin type/color produced for each sample is indicated individually (A–I). Based on PC 1 loadings within each sample category, we hypothesize different susceptibility to diagenetic alteration across the color categories from most to least stable: black, iridescent, mixed visceral organ melanin/gray (i.e., intermediate compositions of eu- and pheomelanin), and brown (J). The 300°C sediment-matured samples are hypothesized to show a reversal of this pattern in PC 1 values, whereby pheomelanin decarbonizes most readily while eumelanin shows more stability.

off, instead directing proteins along hydrolytic reaction pathways. Our PCA further supports this position. The sulfur content of extracted melanin presumably originates from benzothiazole moieties of pheomelanin (Colleary et al. 2015; Roy et al. 2019), whereas that of sediment-matured samples could derive from pheomelanin, unleached keratin breakdown products, and/or from melanoidin-like polymers (Wiemann et al. 2018). PC 3 explains 9.86% of the variation in the dataset (see Supporting Information, Fig. S4A–C, https://doi.org/10.5281/zenodo.7833866), and S-bearing fragments have a sizable net positive loading on PC 3 of either 2.47 or 2.22, depending on the ambiguous identity of the negatively loading fragment with *m/z* 134. Therefore, the only S-bearing fragment(s) with negative loading on PC 3 is large (containing six carbons and a nitrogen), possibly indicating incorporation within a larger polymer through thermal alteration. In contrast, the S-bearing fragments with positive loading on PC 3 are typically smaller, indicating that they are susceptible to volatilization and loss through thermal alteration. Similar PC 3 scores are observed across samples, but with slightly higher values in the sediment-matured feathers relative to the unmatured and capsule-matured melanin extracts as well as the fossils. There may also be a decrease in PC 3 values as temperature increases in sediment maturation, consistent with the loss of volatile S-moieties, but sample sizes are small. The enrichment of more volatile S-bearing moieties in the sediment-matured feathers could be indicative of unleached keratin breakdown products (Saitta et al. 2018b) (e.g., hydrolyzed peptide fragments or free/degraded amino acids) due to (1) a lack of a decay treatment to reduce protein concentrations before maturation or (2) maturation in dry sediment, limiting dissolution of protein breakdown products. S-bearing fragments in sediment-matured feathers could also come from melanoidin-like polymers formed through maturation (Wiemann et al. 2018), again due to high protein and lipid concentrations when no decay has occurred before maturation or dry sediment that could promote condensation reactions. Regardless, this minor discrepancy in PC 3 scores is not solely influenced by S-bearing fragments, used here as a proxy (albeit imperfect due to pheomelanin confounding) for keratin-derived molecules, and would at most explain <10% of the variation in the data. Therefore, we can confidently say that any protein products or melanoidin-like polymers in sediment-matured samples are in low quantities (consistent with observed volume loss in the impressions) and that PCA mostly describes variation in melanin chemistry across our dataset. Similar PC 3 scores between fossils and melanin extracts further highlight that protein loss is natural in fossilization.

Sediment-encased P–T Maturation Simulates Natural Diagenesis and Reveals Key Chemical Transformations of Feather Chemistry.—Animal integumentary structures (e.g., skin, scales, feathers, and hair) are composed of organic mixtures of proteins, lipids (e.g., waxes/oils), and pigments (Morrison et al. 2018). When integumentary structures undergo fossilization, complex organics proceed through multiple taphonomic steps. Comparison of experimental results with fossils in terms of appearance and chemistry suggests that experimental maturation of feathers results in thermobaric decomposition of organics. We hypothesize that, like natural diagenesis, P–T maturation favors hydrolytic loss of integumentary proteins as evidenced by significant volume loss leading to voids/impressions as noted in prior work (Saitta et al. 2018b; Saitta and Vinther 2019).

Lipids such as waxes and triglycerides are predicted to undergo thermally mediated hydrolytic cleavage of ester bonds (e.g.,

https://doi.org/10.1017/pab.2023.11 Published online by Cambridge University Press

TABLE 3. Principal components analysis (PCA) loading matrix showing the loadings for the 55 characteristic time-of-flight secondary ion mass spectrometry (ToF-SIMS) peaks of melanin in PC 1–PC 4 of the total PCA. Peak assignments based on Colleary et al. (2015) and Lindgren et al. (2012, 2014).

Organic series	*m/z*	Fragments	PC 1	PC 2	PC 3	PC 4
Carbon skeletons (C_n^-)	48.001	C_4^-	−0.79348	−0.38106	−0.20128	−0.04774
	72.001	C_6^-	−0.11883	−0.64061	−0.17591	−0.18182
	84.001	C_7^-	0.64412	−0.46335	0.06603	0.26114
	96.001	C_8^-	−0.82092	0.07798	−0.09203	0.08879
	108.001	C_9^-	0.70385	−0.44484	−0.0274	0.05288
Hydrocarbons (C_xH^-)	49.008	C_4H^-	0.07623	−0.81131	0.00647	−0.30771
	61.008	C_5H^-	−0.78069	0.09671	0.14468	0.21807
	73.008	C_6H^-	0.28386	−0.80549	0.11529	−0.20459
	85.008	C_7H^-	0.5136	−0.67589	0.11901	0.10843
	97.008	C_8H^-	0.2648	−0.55265	0.11948	0.05047
	109.008	C_9H^-	0.65874	−0.48373	−0.01573	0.2662
	121.008	$C_{10}H^-$	−0.15281	−0.70235	0.06481	0.21619
	133.008	$C_{11}H^-$	0.60051	−0.1986	0.16582	0.47884
	145.008	$C_{12}H^-$	−0.36019	−0.02106	0.13366	0.1711
	169.008	$C_{14}H^-$	0.68536	−0.17308	0.14279	0.12509
Oxygen bearing ($C_xH_yO_z^-$)	59.014	$C_2H_3O_2^-$	−0.13391	0.06111	0.6239	0.4975
	65.015	C_4HO^-	0.45725	−0.21788	−0.24053	−0.23427
	71.025	$C_3H_3O_2^-$	0.28875	0.06541	0.6588	0.41566
	89.003	C_6HO^-	0.63358	0.32656	−0.29311	−0.12294
	113.003	C_8HO^-	0.23723	0.44589	−0.33622	0.29418
	136.017	$C_7H_4O_3^-$	−0.50253	0.18313	−0.02421	0.02818
	149.003	$C_{11}HO^-$	0.29809	0.39806	0.45738	−0.0744
	160.016	$C_9H_4O_3^-$	0.37889	0.49403	0.2678	0.04476
Nitrogen bearing ($C_xN^-/C_xH_yN^-$)	50.004	C_3N^-	0.649	0.00922	−0.46777	−0.43664
	62.004	C_4N^-	−0.22715	−0.11034	0.29148	0.26806
	63.011	C_4HN^-	−0.71828	0.13035	0.10357	0.09341
	64.019	$C_4H_2N^-$	−0.85863	0.22507	−0.09924	0.03929
	74.004	C_5N^-	0.56919	−0.05277	−0.45536	−0.43887
	86.009	C_6N^-	0.86293	−0.33562	−0.04337	0.12535
	87.011	C_6HN^-	0.5814	−0.0581	0.47945	0.21089
	88.019	$C_6H_2N^-$	0.48274	0.63677	−0.34204	−0.16755
	98.004	C_7N^-	0.79056	−0.12682	−0.23553	−0.24015
	99.011	C_7HN^-	0.45831	0.05401	0.59952	0.38361
	110.004	C_8N^-	0.85731	−0.16372	0.11039	0.18207
	111.011	C_8HN^-	0.79748	0.0315	0.28103	0.13854
	112.019	$C_8H_2N^-$	0.79941	0.09892	0.13855	−0.04169
	122.004	C_9N^-	0.69098	−0.1291	−0.24374	−0.08706
	135.011	$C_{10}HN^-$	0.78599	0.10959	0.04062	0.14465
	146.004	$C_{11}N^-$	0.65979	−0.06678	−0.28121	0.2024
	158.003	$C_{12}N^-$	0.41587	0.17439	−0.51029	0.38937
	159.008	$C_{12}HN^-$	0.44753	0.20384	−0.08908	0.1878
	170.003	$C_{13}N^-$	0.73954	0.29675	−0.11744	0.15208
Nitrogen, sulfur, and oxygen bearing (C_6NSO^-) or nitrogen bearing ($C_{10}N^-$)	134.004/133.971	$C_6NSO^-/C_{10}N^-$	0.54207	−0.04551	−0.24712	0.47626
Nitrogen and oxygen bearing (C_xNO^-)	65.999	C_3NO^-	0.23182	0.47289	−0.49582	0.32742
	89.999	C_5NO^-	0.37084	0.51547	−0.61127	0.24936
	113.999	C_7NO^-	0.74257	0.3612	−0.13423	0.25427
	149.999	$C_{10}NO^-$	0.08715	0.32015	0.39224	0.49388
Nitrogen and sulfur bearing (C_xNS^-)	57.976	CNS^-	0.39801	0.37143	0.41605	−0.60341
	81.976	C_3SN^-	0.45559	0.4353	0.37392	−0.56889
	105.976	C_5SN^-	0.60254	0.37367	0.2338	−0.32843
	117.976	C_6NS^-	0.41639	0.15956	−0.2036	0.44393
Sulfur bearing ($C_xS_y^-/C_xH_yS^-$)	56.980	C_2HS^-	0.34168	0.22413	0.58716	−0.51734
	80.980	C_4HS^-	0.43053	0.27049	0.48577	−0.49807
	100.004	$C_3S_2^-$	−0.59989	0.28103	0.22565	0.36069
	104.980	C_6HS^-	0.44992	0.00809	0.34848	−0.31165

between hydrophobic fatty acids and hydrophilic glycerol/glycerol phosphate groups [Eglinton and Logan 1991]). After hydrolysis, severed hydrocarbon chains can undergo in situ polymerization to be retained within fossils as insoluble aliphatic hydrocarbons (i.e.,

https://doi.org/10.1017/pab.2023.11 Published online by Cambridge University Press

kerogen) (Stankiewicz et al. 1997; Gupta et al. 2009). PCA distinguishes fossils from modern and experimental (capsule- and sediment-matured) samples. Lower PC 2 values in modern/experimental samples compared with fossils are driven largely by enrichment in hydrocarbons (C_xH^-) in the former, possibly originating from residual fatty acids and labile lipids (e.g., epidermal oils/waxes or melanosome lipid bilayers) in the modern/experimental samples that are depleted in fossils (see Supporting Information, Fig. S5A,B, https://doi.org/10.5281/zenodo.7833866). Labile lipid hydrocarbons could have been lost from fossils during postmortem peroxidation (i.e., early-stage decay) and/or through prolonged late-stage oxidative weathering of kerogen, both of which could be experimentally simulated in future work.

Melanin pigments are thought to have linear heteropolymeric structures, stacked oligomeric structures, or a combination of both (Watt et al. 2009), and have been shown to be resistant to hydrolysis, except under harsh alkaline or acidic conditions (Ito et al. 2013). Multiple lines of evidence suggest that increasing PC 1 scores correlate with increasing P–T alteration consistent with diagenesis: (1) At fixed pressure, PC 1 scores increase with increasing maturation temperature; (2) open systems (i.e., sediment-encased maturation) are shifted to higher PC 1 scores; (3) non-hydrocarbon, especially N/S-bearing fragments heavily load PC 1 (e.g., $C_xS_y^-$, $C_xH_yS^-$, C_xN^-, C_xHN^-, C_xNS^-, C_xNO^-, C_xNSO^-) (Fig. 3B, Supporting Information, Fig. S2, https://doi.org/10.5281/zenodo.7833866), where certain smaller fragments (i.e., volatiles) have negative loading, while large fragments (i.e., components of polymers) have positive loading. When fragment masses were plotted against PC 1 loading (Fig. 4), positive loading of large fragments and negative loading of small fragments (for bar plots of PC 1 loadings, see also Supporting Information Fig. S3, https://doi.org/10.5281/zenodo.7833866) suggest that these small volatiles are progressively lost during maturation, whereas larger moieties are enriched at higher temperatures through polymerization. Unmatured melanin extracts with the lowest PC 1 scores are the least altered and enriched in only certain small fragments compared with matured samples and fossils. Capsule-matured melanin extracts have lower PC 1 scores compared with sediment-matured feathers at the same temperature, most likely because they are enriched in those small fragments (i.e., the closed system traps volatiles/labile products otherwise lost in the selectively open system employed by sediment-encased maturation). These observations agree with previously published trends (Colleary et al. 2015; Clements et al. 2016) and suggest that loss of certain volatile/labile moieties concurrent with polymerization/cross-linking occurs during melanin diagenesis, especially with respect to reactive heteroatomic compounds such as N/S-bearing compounds. Similar cross-linking is also reported in maturation experiments on synthetically prepared eumelanin with differing dihydroxyindole and dihydroxyindole carboxylic acid units (Jarenmark et al. 2021). We hypothesize that melanin undergoes thermal decomposition in several overlapping steps (i.e., volatile loss and polymerization co-occur, but different processes potentially dominate at different temperatures). Certain volatile/labile N/S/O-bearing compounds are lost, as evidenced by smaller to larger secondary ion mass with both increased maturation temperature and increased system openness. Additionally, thermal cross-linking of eumelanin monomers (i.e., dihydroxyindoles and dihydroxyindole carboxylic acids) and oligomerization of pheomelanin benzothiazole units are expected to occur (Greco et al. 2011; Ito et al. 2013; Vinther 2020). We infer this in our experiments from the dark stains left on the bentonite matrix (190°C–225°C).

Finally, significant thermal decomposition of melanin (i.e., chemical breakdown/alteration of the polymer) occurs at higher temperatures, leading to carbonization/charring (carbonization point) followed by decarbonization/oxidation around 300°C for eumelanin and even lower (e.g., closer to 250°C) for pheomelanin. In sediment-matured feathers, pheomelanin-dominated samples (i.e., reddish-brown and gray) start to show signs of stain fading at 250°C, whereas eumelanin-dominated samples (i.e., black and iridescent) do so by 300°C. PCA

https://doi.org/10.1017/pab.2023.11 Published online by Cambridge University Press

shows very high thermal alteration and enrichment of polymers at 250°C followed by reversal toward the PC 1 origin as well as increased variability of chemical composition between feathers at 300°C, consistent with increased carbonization/charring followed by decarbonization/oxidation, leading first to carbon-rich then organic-depleted samples (Fig. 3). We posit that black and iridescent feather stains (primarily eumelanic) can survive harsher temperature regimes compared with brown and gray feathers (bearing a mixture of eu- and pheomelanin). The observations of (1) stain retention at higher temperatures for eumelanic feathers, (2) possible trends in PC 1 scores according to melanin content within each treatment/sample category (Fig. 5), and (3) apparent reversal of this pattern at 300°C (Fig. 5) suggest that that eumelanin has higher diagenetic stability than pheomelanin. Intermediate positions occupied by mixed/internal organ melanin and gray colors along PC 1 would suggest an intermediate composition and maturation stability, consistent with other studies (McGraw et al. 2004; Simon and Peles 2010; Liu et al. 2014).

Implications for Paleocolor Reconstruction and Paleobiology of Vertebrates at Large.—The ultimate goal of maturation setups is to simulate natural diagenesis in the laboratory by producing matured soft tissues that are structurally and chemically comparable to fossilized soft tissues. This allows us to chart the basic events in natural diagenesis that modify macro- and microanatomy and the chemistry of the constituent molecules of soft tissues. Additionally, maturation setups more closely simulating natural conditions provide the opportunity to identify key points in diagenesis that lead to information loss or introduce taphonomic biases in our effort to answer prominent paleobiological questions (e.g., inferences of visual signaling, habitat choice, and physiology based on paleocolor).

Our setup and methodology (Fig. 1) simulate diagenesis of biomolecules in a naturalistic, selectively porous clay matrix. This expands the scope of maturation studies, because our experimental samples are more directly comparable to natural fossils both visually and chemically—an improvement over previous studies involving completely open or completely closed experimental systems (McNamara et al. 2013; Colleary et al. 2015). Our results reveal a correlation between macroscopic staining from melanized tissues and broad trends in chemical transformation of melanin (eu-, pheo-, and mixed) through different pressure–temperature regimes. We also identify the temperature-dependent stages of melanin diagenesis and the points where we lose valuable information used in fossil color reconstruction. Our results support the recommendation that fossil melanin samples can be partly characterized by comparing their relative degree of organic staining (as in Fig. 1, although this assumes equal weathering) and the chemistry of N/S-bearing moieties that load PC 1 of our PCA (Fig. 3A,B, Table 3), especially when melanosome shape is rendered indiscernible by diagenesis and/or oxidative weathering, to better inform paleocolor research. Our hope is that this study might widen the scope of fossils amenable for paleocolor reconstruction to test hypotheses relating to the habitat, physiology, and behavior of ancient animals.

Future Directions of Artificial Maturation.—The current setup yields encouraging results: it produces samples that closely mimic the macroscopic staining and key aspects of diagenetic chemical signatures found in fossils in a naturalistic matrix. In producing robust results using samples with minimal treatment/preparation, our protocol also provides a method for deciphering other diagenetic pathways of non-melanin pigments and biomolecules. However, future optimizations could further enhance experimental performance. The original orientation of melanosome layers in experimental samples (e.g., in structurally iridescent arrays) was previously shown be altered through the current two-step setup that mechanically compacts samples first and then proceeds to maturation (Saitta et al. 2018b). To minimize this, future experiments should mechanically compact and thermally mature samples simultaneously.

Future work will also involve experimenting with different gases, such as low oxygen or inert gases, to determine whether similarity to fossils (which would have likely experienced low, but not necessarily zero oxygen

https://doi.org/10.1017/pab.2023.11 Published online by Cambridge University Press

during their history) can be further improved. The minor chemical variation we observed between modern/experimental samples and fossils is most likely due to lipid loss during early decay or late oxidative weathering. This can be remedied by adding pre-maturation decay treatments and/or subjecting samples to oxidation after maturation using warm, moist, oxygenated air. Temperature can fluctuate by 2°C–5°C inside the sample chamber of the current maturation rig, although this is of minimal concern when examining samples across a wide temperature range (190°C–300°C). Future experiments could adjust the chamber design to reduce these temperature fluctuations.

Acknowledgments

We thank C. Colleary (Cleveland Museum of Natural History, Cleveland, OH, U.S.A) for sharing ToF-SIMS data of fossils as well as data of fresh and capsule-matured melanin extract. We also thank A. Shinya (Field Museum of Natural History, Chicago, IL, U.S.A) for her assistance in preparing a few of the sediment-encased maturation samples that did not initially split cleanly. We thank J. Vinther (University of Bristol, Bristol, U.K.) for assistance in obtaining feather samples, discussion on feather maturation experimentation, and for his collaboration that led to the first-generation setup reported by Saitta et al. (2018b). We thank M. J. Benton (University of Bristol, Bristol, U.K.) and J. R. Ali (The University of Hong Kong) for their comments during the conversion of this work from a Ph.D. thesis chapter to an article. Kind thanks to P. Sjövall, Research Institutes of Sweden (RISE), Borås, Sweden, for providing us reference α- and β-keratin ToF-SIMS spectra from Schweitzer et al. (2018). We would also like to thank L. T. Weng (Materials Characterization and Preparation Facility, Hong Kong University of Science and Technology) for running ToF-SIMS on our samples and X. Wang and X. Zheng (Shandong Tianyu Museum of Nature, Pingyi, China; Institute of Geology and Paleontology, Linyi University, China) for fossil feather samples from the pennaraptoran dinosaurs *Yi qi* (STM 31-2) and *Sapeornis* (STM 15-18). A.R. was supported by Hong Kong Ph.D. Fellowship (grant no. HKPF PF16-09281) and the Palaeontological Association (U.K.) Career Development Grant (grant no. PA-CD202103). M.P. and T.G.K. were supported by the HK Research Grant Council General Research Fund (grant no. 17120920). E.T.S. was supported the Bob Savage memorial fund (University of Bristol, U.K.).

Declaration of Competing Interests

The authors declare they have no competing interests.

Data Availability Statement

Supplementary Data contains two files: (1) Supporting Information and (2) Supporting Data PCA worksheet. Both are available from the Zenodo Digital Repository: https://doi.org/10.5281/zenodo.7833866.

Literature Cited

Babarović, F., M. N. Puttick, M. Zaher, E. Learmonth, E. J. Gallimore, F. M. Smithwick, G. Mayr, and J. Vinther. 2019. Characterization of melanosomes involved in the production of non-iridescent structural feather colours and their detection in the fossil record. Journal of the Royal Society Interface 16:20180921.

Brown, C. M., D. M. Henderson, J. Vinther, I. Fletcher, A. Sistiaga, J. Herrera, and R. E. Summons. 2017. An exceptionally preserved three-dimensional armored dinosaur reveals insights into coloration and cretaceous predator-prey dynamics. Current Biology 27:2514–2521 e3.

Burley, N., G. Krantzberg, and P. Radman. 1982. Influence of colour-banding on the conspecific preferences of zebra finches. Animal Behaviour 30:444–455.

Butcher, G. S., and S. Rohwer. 1989. The evolution of conspicuous and distinctive coloration for communication in birds. Pp. 51–108 *in* D. M. Power, ed. Current ornithology, Vol. 6. Springer, Boston.

Carney, R. M., J. Vinther, M. D. Shawkey, L. D'Alba, and J. Ackermann. 2012. New evidence on the colour and nature of the isolated *Archaeopteryx* feather. Nature Communications 3:637.

Cincotta, A., T. T. Nguyen Tu, J. L. Colaux, G. Terwagne, S. Derenne, P. Godefroit, R. Carleer, C. Anquetil, J. Yans, and R. Sansom. 2020. Chemical preservation of tail feathers from *Anchiornis huxleyi*, a theropod dinosaur from the Tiaojishan Formation (Upper Jurassic, China). Palaeontology 63:841–863.

Clements, T., A. Dolocan, P. Martin, M. A. Purnell, J. Vinther, and S. E. Gabbott. 2016. The eyes of *Tullimonstrum* reveal a vertebrate affinity. Nature 532:500–503.

Colleary, C., A. Dolocan, J. Gardner, S. Singh, M. Wuttke, R. Rabenstein, J. Habersetzer, S. Schaal, M. Feseha, M. Clemens, B. F. Jacobs, E. D. Currano, L. L. Jacobs, R. L. Sylvestersen, S. E. Gabbott, and J. Vinther. 2015. Chemical, experimental, and morphological evidence for diagenetically altered melanin in exceptionally preserved fossils. Proceedings of the National Academy of Sciences USA 112:12592–12597.

https://doi.org/10.1017/pab.2023.11 Published online by Cambridge University Press

Cordella, C. B. Y. 2012. PCA: the basic building block of chemometrics. Analytical Chemistry 47. https://doi.org/10.5772/51429.

Cuthill, I. C., W. L. Allen, K. Arbuckle, B. Caspers, G. Chaplin, M. E. Hauber, G. E. Hill, N. G. Jablonski, C. D. Jiggins, and A. Kelber. 2017. The biology of color. Science 357:eaan0221.

de Souza Carvalho, I., F. E. Novas, F. L. Agnolín, M. P. Isasi, F. I. Freitas, and J. A. Andrade. 2015. A Mesozoic bird from Gondwana preserving feathers. Nature Communications 6:1–5.

Eglinton, G., and G. A. Logan. 1991. Molecular preservation. Philosophical Transactions of the Royal Society of London B 333:315–327; discussion 327–328.

Eliason, C. M., and J. A. Clarke. 2018. Metabolic physiology explains macroevolutionary trends in the melanic colour system across amniotes. Proceedings of the Royal Society of London B 285:20182014.

Eliason, C. M., M. D. Shawkey, and J. A. Clarke. 2016. Evolutionary shifts in the melanin-based color system of birds. Evolution 70:445–455.

Fabbri, M., J. Wiemann, F. Manucci, and D. E. Briggs. 2019. Three-dimensional soft tissue preservation revealed in the skin of a non-avian dinosaur. Palaeontology 63:185–193.

Field, D. J., L. D'Alba, J. Vinther, S. M. Webb, W. Gearty, and M. D. Shawkey. 2013. Melanin concentration gradients in modern and fossil feathers. PLoS ONE 8:e59451.

Glass, K., S. Ito, P. R. Wilby, T. Sota, A. Nakamura, C. R. Bowers, K. E. Miller, S. Dutta, R. E. Summons, D. E. G. Briggs, K. Wakamatsu, and J. D. Simon. 2013. Impact of diagenesis and maturation on the survival of eumelanin in the fossil record. Organic Geochemistry 64:29–37.

Goldberg, K., J. O. Menezes, and M. B. Gonzalez. 2017. Geochemistry and Organic Petrography of Aptian-Albian Source Rocks in the Araripe Basin, Northeastern Brazil. AAPG Annual Convention and Exhibition, Houston, TX, April 2–5, 2017.

Greco, G., L. Panzella, L. Verotta, M. d'Ischia, and A. Napolitano. 2011. Uncovering the structure of human red hair pheomelanin: benzothiazolylthiazinodihydroisoquinolines as key building blocks. Journal of Natural Products 74:675–682.

Gupta, N. S., G. D. Cody, O. E. Tetlie, D. E. Briggs, and R. E. Summons. 2009. Rapid incorporation of lipids into macromolecules during experimental decay of invertebrates: initiation of geopolymer formation. Organic Geochemistry 40:589–594.

Hill, G. E., and K. J. McGraw. 2006. Bird coloration: mechanisms and measurements. Harvard University Press, Cambridge, Mass.

Hodge, J. E. 1953. Dehydrated foods, chemistry of browning reactions in model systems. Journal of Agricultural and Food Chemistry 1:928–943.

Ito, S., and K. Wakamatsu. 1998. Chemical degradation of melanins: application to identification of dopamine-melanin. Pigment Cell Research 11:120–126.

Ito, S., K. Wakamatsu, K. Glass, and J. D. Simon. 2013. High-performance liquid chromatography estimation of cross-linking of dihydroxyindole moiety in eumelanin. Analytical Biochemistry 434:221–225.

Jarenmark, M., P. Sjövall, S. Ito, K. Wakamatsu, and J. Lindgren. 2021. Chemical evaluation of eumelanin maturation by ToF-SIMS and alkaline peroxide oxidation HPLC analysis. International Journal of Molecular Sciences 22:161.

Kundrát, M., T. H. Rich, J. Lindgren, P. Sjövall, P. Vickers-Rich, L. M. Chiappe, and B. P. Kear. 2020. A polar dinosaur feather assemblage from Australia. Gondwana Research 80:1–11.

Li, Q., K. Q. Gao, J. Vinther, M. D. Shawkey, J. A. Clarke, L. D'Alba, Q. Meng, D. E. Briggs, and R. O. Prum. 2010. Plumage color patterns of an extinct dinosaur. Science 327:1369–1372.

Li, Y., Z. Song, X.-x. Cao, and S. C. George. 2016. Sedimentary organic matter record of Early Cretaceous environmental changes in western Liaoning Province, NE China. Organic Geochemistry 98:54–65.

Lindgren, J., M. W. Caldwell, T. Konishi, and L. M. Chiappe. 2010. Convergent evolution in aquatic tetrapods: insights from an exceptional fossil mosasaur. PLoS ONE 5:e11998.

Lindgren, J., P. Uvdal, P. Sjovall, D. E. Nilsson, A. Engdahl, B. P. Schultz, and V. Thiel. 2012. Molecular preservation of the pigment melanin in fossil melanosomes. Nature Communications 3:824.

Lindgren, J., P. Sjovall, R. M. Carney, P. Uvdal, J. A. Gren, G. Dyke, B. P. Schultz, M. D. Shawkey, K. R. Barnes, and M. J. Polcyn. 2014. Skin pigmentation provides evidence of convergent melanism in extinct marine reptiles. Nature 506:484–488.

Lindgren, J., P. Sjövall, V. Thiel, W. Zheng, S. Ito, K. Wakamatsu, R. Hauff, B. P. Kear, A. Engdahl, and C. Alwmark. 2018. Soft-tissue evidence for homeothermy and crypsis in a Jurassic ichthyosaur. Nature 564:359.

Littke, R., H. Rotzal, D. Leythaeuser, and D. Baker. 1991. Lower Toarcian Posidonia Shale in southern Germany (Schwäbische Alb). Organic facies, depositional environment, and maturity. Erdöl und Kohle, Erdgas, Petrochemie vereinigt mit Brennstoff-Chemie 44:407–414.

Liu, S. Y., M. D. Shawkey, D. Parkinson, T. P. Troy, and M. Ahmed. 2014. Elucidation of the chemical composition of avian melanin. RSC Advances 4:40396–40399.

Liu, Y., V. R. Kempf, J. Brian Nofsinger, E. E. Weinert, M. Rudnicki, K. Wakamatsu, S. Ito, and J. D. Simon. 2003. Comparison of the structural and physical properties of human hair eumelanin following enzymatic or acid/base extraction. Pigment Cell Research 16:355–365.

Kaye, T. G., M. Pittman, G. Mayr, D. Schwarz, and X. Xu. 2019. Detection of lost calamus challenges identity of isolated *Archaeopteryx* feather. Scientific Reports 9:1182.

Marshall, C. P., G. L. Mar, R. S. Nicoll, and M. A. Wilson. 2001. Organic geochemistry of artificially matured conodonts. Organic Geochemistry 32:1055–1071.

McGraw, K. J., K. Wakamatsu, A. B. Clark, and K. Yasukawa. 2004. Red-winged blackbirds Agelaius phoeniceus use carotenoid and melanin pigments to color their epaulets. Journal of Avian Biology 35:543–550.

McNamara, M., V. Rossi, T. Slater, C. Rogers, A.-L. Ducrest, S. Dubey, and A. Roulin. 2021. Decoding the evolution of melanin in vertebrates. Trends in Ecology and Evolution 36:430–443.

McNamara, M. E., D. E. Briggs, P. J. Orr, D. J. Field, and Z. Wang. 2013. Experimental maturation of feathers: implications for reconstructions of fossil feather colour. Biology Letters 9:20130184.

McNamara, M. E., B. E. van Dongen, N. P. Lockyer, I. D. Bull, and P. J. Orr. 2016. Fossilization of melanosomes via sulfurization. Palaeontology 59:337–350.

McNamara, M. E., J. S. Kaye, M. J. Benton, P. J. Orr, V. Rossi, S. Ito, and K. Wakamatsu. 2018. Non-integumentary melanosomes can bias reconstructions of the colours of fossil vertebrates. Nature Communications 9:2878.

Melenevskii, V. N. 2012. Modeling of catagenetic transformation of organic matter from a Riphean mudstone in hydrous pyrolysis experiments: biomarker data. Geochemistry International 50:425–436.

Michels, R., and P. Landais. 1994. Artificial coalification: comparison of confined pyrolysis and hydrous pyrolysis. Fuel 73:1691–1696.

Morrison, M. L., A. D. Rodewald, G. Voelker, M. R. Colón, and J. F. Prather. 2018. Ornithology: foundation, analysis, and application. Johns Hopkins University Press, Baltimore, Md.

Moyer, A. E., W. Zheng, E. A. Johnson, M. C. Lamanna, D. Q. Li, K. J. Lacovara, and M. H. Schweitzer. 2014. Melanosomes or microbes: testing an alternative hypothesis for the origin of microbodies in fossil feathers. Scientific Reports 4:4233.

https://doi.org/10.1017/pab.2023.11 Published online by Cambridge University Press

Nordén, K. K., J. Faber, F. Babarović, T. L. Stubbs, T. Selly, J. D. Schiffbauer, P. Peharec Štefanić, G. Mayr, F. M. Smithwick, and J. Vinther. 2018. Melanosome diversity and convergence in the evolution of iridescent avian feathers—implications for paleocolor reconstruction. Evolution 73:15–27.

Parry, L. A., F. Smithwick, K. K. Nordén, E. T. Saitta, J. Lozano-Fernandez, A. R. Tanner, J. B. Caron, G. D. Edgecombe, D. E. Briggs, and J. Vinther. 2018. Soft-bodied fossils are not simply rotten carcasses—toward a holistic understanding of exceptional fossil preservation: exceptional fossil preservation is complex and involves the interplay of numerous biological and geological processes. Bioessays 40:1700167.

Pinheiro, F. L., G. Prado, S. Ito, J. D. Simon, K. Wakamatsu, L. E. Anelli, J. A. Andrade, and K. Glass. 2019. Chemical characterization of pterosaur melanin challenges color inferences in extinct animals. Scientific Reports 9:1–8.

Prauss, M., B. Ligouis, and H. Luterbacher. 1991. Organic matter and palynomorphs in the 'Posidonienschiefer'(Toarcian, Lower Jurassic) of southern Germany. Geological Society of London Special Publication 58:335–351.

Purnell, M. A., P. J. C. Donoghue, S. E. Gabbott, M. E. McNamara, D. J. E. Murdock, R. S. Sansom, and A. Smith. 2018. Experimental analysis of soft-tissue fossilization: opening the black box. Palaeontology 61:317–323.

Roulin, A. 2014. Melanin-based colour polymorphism responding to climate change. Global Change Biology 20:3344–3350.

Roy, A., M. Pittman, E. T. Saitta, T. G. Kaye, and X. Xu. 2019. Recent advances in amniote palaeocolour reconstruction and a framework for future research. Biological Reviews of the Cambridge Philosophical Society 95:22–50.

Saitta, E., and J. Vinther. 2019. A perspective on the evidence for keratin protein preservation in fossils: an issue of replication versus validation. Palaeontologia Electronica. https://doi.org/10.26879/1017E.

Saitta, E. T., C. Rogers, R. A. Brooker, G. D. Abbott, S. Kumar, S. S. O'Reilly, P. Donohoe, S. Dutta, R. E. Summons, and J. Vinther. 2017. Low fossilization potential of keratin protein revealed by experimental taphonomy. Palaeontology 60:547–556.

Saitta, E. T., I. Fletcher, P. Martin, M. Pittman, T. G. Kaye, L. D. True, M. A. Norell, G. D. Abbott, R. E. Summons, K. Penkman, and J. Vinther. 2018a. Preservation of feather fibers from the Late Cretaceous dinosaur *Shuvuuia deserti* raises concern about immunohistochemical analyses on fossils. Organic Geochemistry 125:142–151.

Saitta, E. T., T. G. Kaye, and J. Vinther. 2018b. Sediment-encased maturation: a novel method for simulating diagenesis in organic fossil preservation. Palaeontology 62:135–150.

Schweitzer, M. H., W. Zheng, A. E. Moyer, P. Sjövall, and J. Lindgren. 2018. Preservation potential of keratin in deep time. PLoS ONE 13:e0206569.

Simon, J. D., and D. N. Peles. 2010. The red and the black. Accounts of Chemical Research 43:1452–1460.

Slater, T. S., M. E. McNamara, P. J. Orr, T. B. Foley, S. Ito, and K. Wakamatsu. 2020. Taphonomic experiments resolve controls on the preservation of melanosomes and keratinous tissues in feathers. Palaeontology 63:103–115.

Smithwick, F. M., R. Nicholls, I. C. Cuthill, and J. Vinther. 2017. Countershading and stripes in the theropod dinosaur *Sinosauropteryx* reveal heterogeneous habitats in the Early Cretaceous Jehol Biota. Current Biology 27:3337–3343.e2.

Stankiewicz, B. A., J. C. Hutchins, R. Thomson, D. E. Briggs, and R. P. Evershed. 1997. Assessment of bog-body tissue preservation by pyrolysis-gas chromatography/mass spectrometry. Rapid Communications in Mass Spectrometry 11:1884–1890.

Tesfaye, T., B. Sithole, D. Ramjugernath, and V. Chunilall. 2017. Valorisation of chicken feathers: characterisation of chemical properties. Waste Management 68:626–635.

Thomas, D. B., P. C. Nascimbene, C. J. Dove, D. A. Grimaldi, and H. F. James. 2014. Seeking carotenoid pigments in amber-preserved fossil feathers. Scientific Reports 4:5226.

Vinther, J. 2020. Reconstructing vertebrate paleocolor. Annual Review of Earth and Planetary Sciences 48:345–375.

Vinther, J., D. E. Briggs, R. O. Prum, and V. Saranathan. 2008. The colour of fossil feathers. Biology Letters 4:522–525.

Vinther, J., R. Nicholls, S. Lautenschlager, M. Pittman, T. G. Kaye, E. Rayfield, G. Mayr, and I. C. Cuthill. 2016. 3D camouflage in an ornithischian dinosaur. Current Biology 26:2456–2462.

Vitek, N. S., J. Vinther, J. D. Schiffbauer, D. E. Briggs, and R. O. Prum. 2013. Exceptional three-dimensional preservation and coloration of an originally iridescent fossil feather from the Middle Eocene Messel Oil Shale. Paläontologische Zeitschrift 87:493–503.

Watt, A. A. R., J. P. Bothma, and P. Meredith. 2009. The supramolecular structure of melanin. Soft Matter 5:3754–3760.

Wiemann, J., M. Fabbri, T.-R. Yang, K. Stein, P. M. Sander, M. A. Norell, and D. E. Briggs. 2018. Fossilization transforms vertebrate hard tissue proteins into N-heterocyclic polymers. Nature Communications 9:4741.

Wiemann, J., J. M. Crawford, and D. E. G. Briggs. 2020. Phylogenetic and physiological signals in metazoan fossil biomolecules. Science Advances 6:eaba6883.

Yang, Z., B. Jiang, M. E. McNamara, S. L. Kearns, M. Pittman, T. G. Kaye, P. J. Orr, X. Xu, and M. Benton. 2019. Pterosaur integumentary structures with complex feather-like branching. Nature Ecology and Evolution 3:24.

Zhang, F., S. L. Kearns, P. J. Orr, M. J. Benton, Z. Zhou, D. Johnson, X. Xu, and X. Wang. 2010. Fossilized melanosomes and the colour of Cretaceous dinosaurs and birds. Nature 463:1075–1078.

https://doi.org/10.1017/pab.2023.11 Published online by Cambridge University Press